Fully microscopic model of 200 MeV proton-^{12}C elastic and inelastic scattering

S. Karataglidis, P. J. Dortmans, K. Amos, and R. de Swiniarski*
School of Physics, University of Melbourne, Parkville 3052, Victoria, Australia
(Received 7 April 1995)

An effective two nucleon (NN) interaction in the nuclear medium is defined from an accurate mapping of the $NN\,g$ matrices obtained by solving the Brueckner-Bethe-Goldstone equations for infinite nuclear matter. That effective interaction is used in a fully microscopic calculation of the nonlocal effective proton-^{12}C interaction from which we obtain predictions of the differential cross section and analyzing power for 200 MeV elastic scattering. The relative motion wave functions so found are used as the distorted waves in a distorted wave approximation (DWA) study of select inelastic scattering events. The effective NN interaction is used as the transition operator in those calculations. The relevant nuclear spectroscopy for the elastic and DWA (p,p') calculations is found from a full $(0+2)\hbar\omega$ shell model evaluation of the positive parity states while a restricted $(1+3)\hbar\omega$ shell model space has been used to give the negative parity states. Results are compared with those of the $0p$-shell model of Cohen and Kurath or with those based upon axially symmetric, projected Hartree-Fock calculations. The diverse structure model wave functions are assessed by using them in calculations to compare with measured longitudinal, transverse electric, and transverse magnetic form factors from electron scattering to many of the excited states of ^{12}C. Using those models of the structure of ^{12}C in our completely microscopic model of the elastic and inelastic scattering of 200 MeV protons, good fits have been found to the cross section and analyzing power data.

PACS number(s): 25.40.Cm, 25.40.Ep, 21.30.+y, 24.10.Ht

I. INTRODUCTION

Understanding the nature and specifics of the potential energy of interaction between two colliding nuclei is central in almost all studies of their possible reactions. Conventionally, elastic scattering data are used as measures to assess any candidate form of such (nonrelativistic) interactions. Also it is usual to consider those interactions to have local forms that may be both complex and energy dependent and it is common to use an approximate inverse method by adjusting values of parameters in the chosen forms seeking a result that "best fits" measured data [1].

A proper direct approach, however, is to start with some form of the underlying two nucleon, (NN), g matrices and, without adjustment, to fold them with the density matrices of the colliding systems. The optical potential so defined is nonlocal due to proper antisymmetrization of the projectile and target nucleons and to any nonlocality that may reside in the form used for the NN g matrices. The study of nucleon-nucleus, (NA), scattering then is favored as the antisymmetrization is the least problematic in the theoretical development of the optical potentials for elastic scattering. That is also the case for inelastic scattering transition amplitudes when they are defined within the distorted wave approximation (DWA) and with appropriate large basis (microscopic) structure wave functions. To date, few if any calculations have been made observing such a strict definition of a fully microscopic description of NA scattering. Herein we attempt to do so with an analysis of the scattering of 200 MeV protons from ^{12}C.

The elastic and inelastic scattering data of protons from ^{12}C are particularly useful to study in a quest for the "best" effective NN and NA interactions at medium energies. First there are many states below 20 MeV in excitation and which can be resolved easily for any incident energy to 800 MeV. Second, those states include both negative and positive parity ones as well as involving both natural and unnatural spin-parity transitions (from the ground state) and for both possible isospin transfer values. Further there are much high quality scattering data available, especially cross sections and analyzing powers. Also there are considerable data on the electron scattering form factors against which the chosen models of structure can be tested. Finally, the target is light enough that reasonable large basis models of its structure can be made for use in scattering analyses.

In this paper we have chosen to study the 200 MeV data of Comfort *et al.* [2]; data that have a special interest for us. This energy lies in a "transition" region between low and intermediate energies in which one expects [3,4] not only effects of nonlocalities in the effective NA interaction but also density dependent effects in the NN effective interaction upon which that NA interaction is built, will be important. Furthermore, these 200 MeV data, and others in the energy range 120–185 MeV [5], have been analyzed in the past with a diverse set of postulates about the reaction process and with a number of different effective interaction prescriptions. Most of those data have been analyzed in the nonrelativistic

*On leave from the Institut des Sciences Nucléaires, IN2P3 et Université J. Fourier, 38026 Grenoble–Cedex, France.

distorted wave approximation (DWA) and usually with either the Love-Franey (LF) [6,7] or the Hamburg [4] effective interaction. Those analyses have been considered to be "microscopic" but they are really at best semimicroscopic given the strict definition we have set above. In all cases the distorted waves were generated using a local and phenomenological model of the optical potential and the transition operators, while predicated upon the NN scattering properties, were adjusted in line with various DWA calculation results.

In most calculations of inelastic scattering the input spectroscopy is quite limited. For the positive parity states in ^{12}C, the Cohen and Kurath (CK) 0p-shell model [8] has been used while the negative parity states were obtained from the Millener and Kurath (MK) psd-shell model [9]. With such limited basis structure and at higher energies, recent analyses of proton-^{12}C inelastic scattering (from 200 to 800 MeV) [10] with the latest energy dependent LF force gave quite good results for the cross sections but the analyzing powers were not well described. However in those calculations adjustments had to be made for each transition even to fit the cross sections. Core polarization corrections were needed to give the observed magnitudes and the single particle bound state wave functions were varied to give the best agreement with the shape of the data. Also relativistic effects must grow in importance with such a range of energies as has been shown by coupled channel analyses of the strong, collectivelike transitions [11]. That study, based upon the Dirac equation, gave better fits to the measured data from 200 to 800 MeV than were found with any of the nonrelativistic treatments. The fits to both the cross sections and to the analyzing powers from the coupling of the 0^+, 2^+, and 4^+ states using the collective model are exceptionally good [12]. An ultimate aim of our fully microscopic approach is to achieve equivalent fits to the measured results. Currently we are limited to using the DWA given that inclusion of channel coupling in a microscopic approach is orders of magnitude more complex, at least from the viewpoint of computation. Our studies are based upon nonrelativistic theory but we have used relativistic kinematics in the optical potential calculations of elastic scattering and in the DWA analyses of inelastic transition data.

Within the distorted wave theories there are three basic ingredients that must be specified to calculate inelastic scattering probability amplitudes. They are the optical potentials from which the distorted waves themselves are to be generated, the effective NN interaction that promotes each transition, and the structure information of both single nucleon bound states and the many nucleon target wave functions.

Given that the NN g matrices are most easily specified in momentum space, attempts have been made [13,14] to analyze nucleon-nucleus (NA) elastic scattering with a momentum space solution of the Schrödinger equation. But as yet there are no programs to use the resulting wave functions to analyze other reaction data. Thus, as part of this study is to investigate a select set of inelastic transitions as well as the elastic event, we have chosen to work with coordinate space solutions. The program DWBA91 of Raynal [15] enables us to generate microscopic optical model potentials from a specified NN effective interaction and to use that same interaction as the transition operator in subsequent DWA studies of inelastic scattering data.

In coordinate space, microscopic model studies of (NA) elastic scattering begin by defining effective interactions to the actual NN g matrices one believes to be responsible for the events. Those effective interactions can have diverse operator character (central, tensor, two body spin orbit, etc.) but always relatively simple local form factors (i.e., sum of Yukawa or Gaussian functions) have been used. Furthermore the exchange amplitudes arising from antisymmetrization in the folding process usually have been approximated to give a local equivalent NA optical potential. Nevertheless, with such an approach, elastic scattering data can be described quite well [4,16]. Until recently, the effective NN interactions used in NA scattering analyses were so determined but then they were modified, often quite seriously, to better describe the NA scattering data. By so doing, the ability to accurately ascribe whether specific effects were due to the fitting of the effective interaction or due to any of the underlying properties of the scattering (the NN interaction, medium effects, nuclear structure, etc.) was lost. Of such forces, the LF effective interaction was based upon the on-shell free NN t matrices (the NN scattering amplitudes) as defined by the Arndt phase shifts [17] giving quite reasonable descriptions of scattering for energies up to 800 MeV. No constraints were applied to the off-energy-shell properties of the t matrices or to allow for medium modifications of those t matrices specifically. That was considered a major limitation [13] although the effective interaction was designed with impulse approximation conditions in mind. A subsequent development of the LF effective interaction treated medium modifications "on the average" but still did not offset nonunitary problems associated with the method of specification [3].

In contrast, the Hamburg force was based upon g matrix elements associated with the Paris interaction [18] and evaluated allowing for Pauli blocking and, very approximately, the average background mean field in which the nucleons move. Those g matrices were cast as functions of relative momenta (for each NN channel) whose Fourier transformations were then mapped against those of an effective (coordinate space) interaction. As with the LF interaction, the Hamburg force was structured to have central, tensor, and spin-orbit characters. Each component had a set of four Yukawa functions as the form factors. The ranges of those Yukawas were chosen *a priori* and their strengths were then adjusted to minimize the integrated squared difference between the values of the original g matrices and those of the effective interaction in the range of momentum transfer up to 5 fm^{-1}. The proton-nucleus optical model potentials were then deduced by folding, and reasonable results were obtained for proton scattering at various energies to 400 MeV from targets ranging between ^{12}C and ^{208}Pb.

However the Hamburg effective interactions do not reproduce sufficiently well the off-shell matrix elements to which they were fit. In particular, they do not give a sat-

isfactory representation of the zero density (free NN), Paris t matrices. That motivated the development of an effective interaction scheme [19,20] to give an equally utilitarian form. In the zero density limit (free NN scattering), this new effective interaction [20] is a good representation of the half-off-shell Paris t matrices (at 200 MeV) for most low-J NN channels. With it and neglecting medium corrections, optical model potentials were found that also led to a reasonable description of the differential scattering cross sections in two test cases: 200 MeV protons from ^{12}C and ^{16}O. But the analyzing power predictions were quite poor. On the other hand, by using an effective interaction that gave comparable fits to the half-off-shell g matrix elements computed with both Pauli blocking and average field effects in the relevant Brueckner-Bethe-Goldstone (BBG) equations, the attendant optical potentials for 200 MeV protons on both nuclei led to better fits to the differential cross section data and very much better ones to the measured analyzing power. The procedure used to obtain that effective interaction [20] has been refined especially in regard to the weight given to fits in select two nucleon channels so that we now have an effective NN interaction for use at 200 MeV whose double Bessel transforms give excellent fits to most low J NN g matrices for 0.5–1.0 fm^{-1} about the "on-shell" value [21]. More details will be given in the next section.

That effective interaction has been used as input to the program DWBA91, first to predict the cross section and analyzing power for the elastic scattering of 200 MeV protons from ^{12}C. To do so also requires that the ground state spectroscopy be defined. This we have obtained with various structure model calculations; structure models that also define the spectroscopy of the excited states that were considered in studies of inelastic scattering. Details of the structure models we have used, the spectra that result, and the electron scattering form factors they yield, are presented in Sec. III.

The elastic scattering problem is solved using the code DWBA91 by folding the effective interaction with the density matrix elements of the ground state and by allowing for antisymmetrization between the projectile and each and every nucleon in the target (all nucleons are "active" in our calculations of ^{12}C), the resulting optical potential has both a local "direct" and a nonlocal "exchange" part. The latter component has been approximated by a local equivalent term in the past, or simply ignored. Specifics of the folding to give the optical potentials we have used are given in Sec. IV along with the results of those calculations.

The same effective interaction, the fully microscopic (nonlocal) optical potentials, and the spectroscopic information from our large basis shell model study (and from others), have all been used in DWA analyses of select inelastic scattering cross sections and analyzing powers. The structures of the relevant excited states have been used to define the optical potentials for the outgoing distorted waves. We report the results of those DWA calculations in Sec. V. Quite different aspects of the effective interaction are important in analyses of such scattering according to the spin parity involved in the transitions. Given that the ground state is a 0^+ state that equates to the spin-parity assignment of the final state. The quality of the various spectroscopic models used varies with transitions and so we have cross correlated the (p,p') assessments with analyses of electron scattering form factors.

II. THE EFFECTIVE INTERACTION

Nonrelativistic many-body theories of the NA optical potentials are framed around the NN t matrices which, in momentum space and for channels $\{JST\}$, are solutions of the Lippmann-Schwinger equation,

$$t^{(JST)}_{LL'}(p',p;k) = V^{(JST)}_{LL'}(p',p) + \frac{2}{\pi}\sum_l \int_0^\infty V^{(JST)}_{Ll}(p',q)\frac{1}{q^2-k^2-i\varepsilon}t^{(JST)}_{lL'}(q,p;k)\ q^2dq\ , \tag{1}$$

with k being the relative on-shell momentum. But when the struck nucleon is embedded in a nuclear medium, it is more appropriate to use medium modified NN g matrices in optical model calculations. The g matrices used herein are solutions of the BBG equation for infinite nuclear matter, i.e., of

$$G^{(JST)}_{LL'}(p',p;k,k_f) = V^{(JST)}_{LL'}(p',p) + \frac{2}{\pi}\sum_l \int_0^\infty V^{(JST)}_{Ll}(p',q)[\mathcal{H}]G^{(JST)}_{lL'}(q,p;k,k_f)\ q^2dq\ , \tag{2}$$

where

$$\mathcal{H}(q,k,K,k_f) = \frac{\bar{Q}(q,K;k_f)}{\bar{E}(q,K;k_f)-\bar{E}(k,K;k_f)-i\varepsilon} \tag{3}$$

in which $\bar{Q}(q,K;k_f)$ is an angle averaged Pauli operator with an average center of mass (c.m.) momentum K being

$$\begin{aligned} K &= K(k;k_f,p_0) \\ &= (k^2+p_0^2)^{\frac{1}{2}} \quad \text{if} \quad 0 \le 2k \le k_f - p_0 \\ &= \{(k^2+p_0^2) - \tfrac{1}{4}\left[(2k+p_0)^2 - k_f^2\right]\}^{\frac{1}{2}} \\ &\quad \text{if } k_f - p_0 \le 2k \le k_f + p_0\ . \end{aligned} \tag{4}$$

This prescription as set by Haftel and Tabakin [22], with

p_0 being the laboratory incident momentum and k_f being the Fermi momentum, is known to be a good approximation. The energies in the propagators of the BBG equations include auxiliary potentials U defined by

$$\bar{E}(q,K;k_f) = \left(\frac{\hbar^2}{m}\right)(q^2+K^2) + U(|\mathbf{q}+\mathbf{K}|) + U(|\mathbf{q}-\mathbf{K}|) \ . \quad (5)$$

Details of the calculations have been given previously [22,23] and the result is tables of complex numbers for each incident energy, Fermi momentum value, and set of relative momenta for each NN channel. In a free NN collision the struck nucleon initially has zero momentum, but when it is embedded in (local) nuclear matter that struck nucleon can have a range of momentum values and the relative and c.m. momenta are not necessarily the same.

With any parameterization scheme to define an effective interaction one must first choose the set of input data for which a fit is to be optimized. The data may be purely real (such as for NN potentials themselves) or complex (such as t or g matrices). One may restrict consideration solely to on-shell or half-off-shell data or one may take fully off-shell information. It is possible even to select a limited set of two body channel information. Herein, the half-off-shell t matrices (and later g matrices) are considered as these are the most pertinent quantities in almost all NN problems. We define the input t matrices as $t^{(JST)}_{LL'}(k',k;E=k^2)$, where J is the total angular momentum of the NN system, S the spin, T the isospin, L and L' the orbital angular momenta, k' the off-shell momenta, and k the on-shell momentum.

Consider a local effective transition matrix in coordinate space and of the form

$$t^{(i)ST}_{\rm eff}(r,E) = \sum_{j=1}^{n_i} S^{(i)}_j(E)\frac{e^{-(r/\lambda^{(i)}_j)}}{r} = \sum_{j=1}^{n_i} S^{(i)}_j(E)\frac{e^{-\mu^{(i)}_j r}}{r} \ , \quad (6)$$

for each operator of the central, tensor and spin-orbit set $(i)=\{C,\ S_{12}\,,$ and $L\cdot S\}$. Therein $S^{(i)}_j(E)$ are complex, energy dependent strengths, $\lambda^{(i)}_j = 1/\mu^{(i)}_j$ are the ranges of the interaction, and j represents the set of ranges chosen. In principle, the number of strengths and ranges (n_i) chosen can be as large as one likes, though for all operators $n_i = 4$ seems to be sufficient for one to reproduce accurately the half-off-shell t matrices for laboratory energies between 50 and 400 MeV [24].

To match data in the $\{JSTLL'\}$ channel form to the effective interaction elements in the ST channel form, the angular momentum state expectation values of the three operators in the effective interactions are needed. Explicitly, those expectation values are given by the set

$$\langle\theta_C\rangle = \delta_{LL'},$$
$$\langle\theta_{L\cdot S}\rangle = \tfrac{1}{2}[J(J+1)-L(L+1)-S(S+1)]\delta_{LL'},$$

and

$$\langle\theta_{S_{12}}\rangle = \begin{cases} 2\delta_{S1} & \text{if } L=J, \\ \frac{-2(J-1)}{(2J+1)} & \text{if } L=L'=J-1, \\ \frac{-2(J+2)}{(2J+1)} & \text{if } L=L'=J+1, \\ \frac{6}{(2J+1)}\sqrt{J(J+1)} & \text{if } L=J\pm1,\ L'=J\mp1\ , \end{cases} \quad (7)$$

and it is possible to obtain the effective coordinate space transition matrix in terms of central, tensor, and spin-orbit components by

$$t^{ST}_{\rm eff}(r,E) = \sum_i \langle\theta_i\rangle\, t^{(i)ST}_{\rm eff}(r,E) \ . \quad (8)$$

With this form of $t^{ST}_{\rm eff}(r,E)$ as the effective interaction, a double Bessel transform determines the equivalent momentum space representation [19,22], viz.,

$$t^{(JST)}_{({\rm eff})LL'}(k',k;E=k^2) = \sum_i \langle\theta_i\rangle \int_0^\infty j_L(k'r)\ t^{(i)ST}_{\rm eff}(r,E)\ j_{L'}(kr)\ r^{2+\lambda}dr$$
$$= \sum_{ij} \langle\theta_i\rangle\ S^{(i)}_j(E) \int_0^\infty j_L(k'r)\left(\frac{e^{-\mu^{(i)}_j r}}{r}\right) j_{L'}(kr)\ r^{2+\lambda}dr$$
$$= \sum_{ij} \langle\theta_i\rangle\ S^{(i)}_j(E)\ \tau^{(JST)}_{LL'}(k',k;\mu^{(i)}_j) \ , \quad (9)$$

where $\lambda = 2$ for tensor states and 0 otherwise.

Assuming that the ranges are independent of energy and momenta (and later of nuclear density), and that the strengths depend only on the energy, the effective representation may be separated into individual sets. The optimal set of ranges and strengths then are those which give a χ^2 minimization of

$$\min := ||t^{(JST)}_{LL'}(k',k;E) - t^{(JST)}_{({\rm eff})LL'}(k',k;E)|| \ . \quad (10)$$

Since it is desirable to have the minimization of the t matrices centered around the on-shell value, we include in the minimization the weighting, $\omega = \exp\{-[(k'-k)^2/\beta^2]\}$, where β is set to 0.3 fm^{-1}. The

process has been used with the g matrices as well so that we have an effective interaction specified in terms of $g_{\rm eff}^{(i)ST}(r;E,k_f)$ where k_f is the Fermi momentum. That Fermi momentum will have a radial variation when these effective g matrices are folded with the density profile of the ^{12}C nucleus. The specific radial variation is defined later.

Optimization of the effective interaction is facilitated by using a two step process. First the ranges, assumed independent of density (Fermi momentum), are determined optimally. One is free, of course, to specify values for any of these ranges. Here we have chosen to do so as previously [19]. To take into account the long-range nature of the pion tail we set $\mu_1^{(C)} = 0.71$ fm^{-1}. We also set the ranges of the tensor and spin-orbit components of the interaction to be the same and limit their long-range nature with $\mu_1^{(L\cdot S)} = 1.25$ fm^{-1}. As for the short-range nature, in all cases we set $\mu_1^{(L\cdot S)} = 4.0$ fm^{-1}, since ranges shorter than this probe regions in which the NN interactions are not well determined or if at all defined. The other ranges were adjusted in various searches to give good representations of the t matrices. The final values used are $\mu_2^{(C)} = 1.758$ fm^{-1}, $\mu_3^{(C)} = 2.949$ fm^{-1}, $\mu_2^{(L\cdot S)} = 2.184$ fm^{-1}, and $\mu_3^{(L\cdot S)} = 3.141$ fm^{-1}. With the ranges fixed, the strengths are then determined at the desired energies and densities for each spin/isospin state by simple mapping techniques. Tables of the interactions used herein (with g matrices found from the Paris interaction in particular) are contained in Ref. [21].

The quality of our mapping procedure is illustrated with the comparisons between the exact and effective interaction (double Bessel transforms) free scattering t matrices that are shown in Figs. 1 and 2. The real and imaginary parts of the half-off-shell t matrices are shown in those, respectively, and for the $^1P_1$, $^1S_0$, $^3S_1$, and $^3P_1$ channels as indicated. At energies of interest,

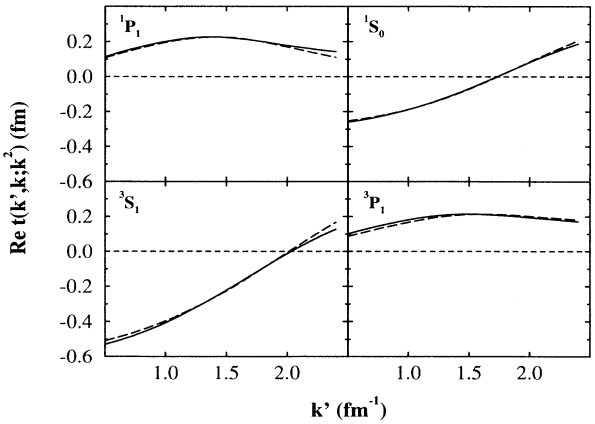

FIG. 1. The real parts of the half-off-shell-NN t matrices built from the Paris [18] interaction at an on-shell momentum of 1.55 fm^{-1} (200 MeV). The actual t matrices are displayed by the solid curves for each of the identified two nucleon angular momentum channels and the dashed curves portray those found by using our "free" effective interaction.

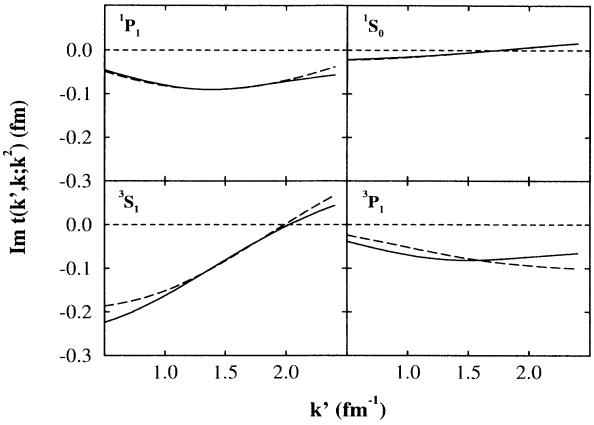

FIG. 2. As for Fig. 1, but for the imaginary parts of the t matrices.

those channels are the dominant terms in the singlet-odd, singlet-even, triplet-even, and triplet-odd two body segments, respectively. The on-shell momentum was taken as 1.55 fm^{-1} since we seek the effective interaction for 200 MeV protons on nuclei. Similar quality of fits were found with the g matrices for the different Fermi momenta (to 1.6 fm^{-1}) needed to define the medium modified specification of the effective interaction. The exact t matrices (of the Paris interaction) are displayed by the solid curves in both diagrams while the dashed curves are the results found from our effective interaction. Clearly, save for the imaginary part of the $^3P_1$ channel, the fits are very good especially for a region around the on-shell point. The imaginary part of the $^3P_1$ t matrix is not very large and the effective interaction result is not so different to the actual one to be of concern. Such results are not dependent upon the precise "realistic" interaction with which one starts. We have found equally good effective interactions to map to the t and g matrix elements obtained starting with the BonnB [25] interaction.

III. SPECTROSCOPY

A. The structure models for ^{12}C

The spectrum of ^{12}C was calculated using the program OXBASH [26] and with the MK3W interaction, which consists of the following statements.

(i) The Cohen and Kurath (8–16)POT interaction [8], for the $0p$ shell matrix elements [although we have modified them to be the (8–16)2BME values in our calculations].

(ii) The Wildenthal interaction as supplied with the program OXBASH [26] for the $0d1s$ shell matrix elements.

(iii) The Millener-Kurath interaction [9] for the (psd)-cross shell elements.

(iv) Those matrix elements, also supplied with the program OXBASH [26], for the other elements spanning the space from the $0s$ to the $0f1p$ shells.

The positive parity states of ^{12}C were calculated in a

complete $(0+2)\hbar\omega$ space using this interaction, while the negative parity states were calculated in a restricted $(1+3)\hbar\omega$ space. In both calculations the same single particle basis of $0s$ up to and including the $0f1p$ shell was used. Hence the restriction from a full $(1+3)\hbar\omega$ study is that we have not included the $0g1d2s$ shell.

The spectrum of ^{12}C so obtained up to 20 MeV in excitation energy is displayed in Fig. 3 wherein it is compared with the experimental values [27], with the spectrum found using a particle-hole model (PHM) [28] based upon a multiconfiguration Hartree-Fock calculation and with that from a standard $0p$-shell model (CK) calculation [8]. The restricted basis of the CK calculation means that only positive parity states result. With exceptions, most notably the $3_1^-;0$ state at 9.64 MeV and the superdeformed $0_1^+;0$ state at 7.65 MeV, our calculated spectrum is in agreement with observation to within 2 MeV, and is a marked improvement on the others, particularly as the PHM calculation places the $2_1^+;0$ (4.44 MeV) state so far from the accepted value.

All established spin-parity assignments are matched by our large basis shell model calculations, and mostly with good agreement for the excitation energies. Of those states for which the spin-parity (and isospin) assignments are uncertain, there is some doubt as to the spin of the 18.35 MeV state. It is listed [27] as being both a $2^-;0+1$ state and a $3^-;1$ state. A 2^- assignment is supported by analyses of pion and proton inelastic scattering data [29], while the 3^- assignment is supported by an analysis of inelastic electron scattering data [30]. However, in that analysis of the longitudinal electron scattering form factor, Yamaguchi *et al.* [30] give the energy of the state as 18.6 MeV. Therefore, the state at 18.35 MeV is more likely a 2^- state. The 13.35 MeV state is listed [27] as a $(2^-);0$ state. However, there is also some doubt about that assignment. Millener [27,31] suggests that it is probably a 4^- state. Both our $(1+3)\hbar\omega$ and the PHM model [28] calculations predict that a $4^-;0$ state lies close to this excitation energy, and that assignment is also supported by a calculation of the alpha decay width of the state [32] that was made using an alpha cluster model for ^{12}C. Detailed microscopic model analyses of the inelastic proton scattering data to the assumed $2^-;0$ states (11.83 MeV, 18.35 MeV) and to the assumed $4^-;0$ 13.35 MeV state are in progress to resolve any residual problem with those assignments.

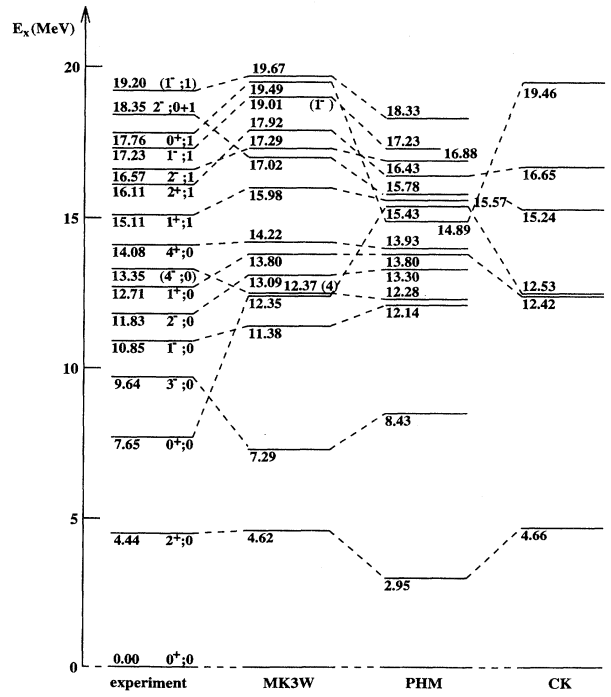

FIG. 3. Energy level diagram for the low-lying states in ^{12}C. The present calculation (MK3W) is compared to experiment [27], as well as the PHM model of Amos *et al.* [28] and the $0p$-shell model of Cohen and Kurath [8].

B. The one body density matrix elements and electron scattering form factors

As a test of the suitability of the calculated nuclear wave functions, and to determine the appropriate single particle wave functions for use in the analyses of the elastic and inelastic proton scattering, elastic and inelastic electron scattering form factors for ^{12}C were analyzed. Our calculations of those form factors were made using the standard prescriptions for them given by de Forest and Walecka [33], but modified for the transverse electric case by the formalism of Friar and Haxton [34] wherein Siegert's theorem is used to account for meson exchange current effects. The resultant effective (one body) transverse electric multipole operators have significant effects when used with $0\hbar\omega$ wave functions [35]. Herein, the $T^{el'}$ operator form [34,35] has been used for the calculation of the transverse electric form factors as that seems to be the most appropriate for calculations using $0\hbar\omega$ wave functions [35]. One body operators have been used also to facilitate calculations of both the longitudinal and transverse magnetic form factors. Consequently, one body density matrix elements (OBDME's) are needed from the structure calculations to evaluate all of the electron scattering form factors.

Those OBDME's (transition densities and shell occupancies) for all the transitions considered herein have been tabulated [35,36]. They are the (singly) reduced matrix elements of an irreducible particle-hole tensor operator formed from the general transition density matrix elements (for protons and neutrons separately),

$$\rho^{m_1 m_2 M_i M_f}_{j_1 j_2 J_i J_f} = \left\langle \Psi_{J_f M_f} \left| a^\dagger_{j_2 m_2}\ a_{j_1 m_1} \right| \Psi_{J_i M_i} \right\rangle , \quad (11)$$

by using

$$a^\dagger_{j_2 m_2} a_{j_1 m_1} = \sum_{I,N} (-1)^{(j_1 - m_1)}\ \langle j_1\, m_1\, j_2\ -m_2 |\, I\ -N\rangle \times \left[a^\dagger_{j_2} \times \tilde{a}_{j_1} \right]^{IN} , \quad (12)$$

so that the Wigner-Eckart theorem gives

$$\rho^{m_1 m_2 M_i M_f}_{j_1 j_2 J_i J_f} = \sum_{I,N} (-1)^{(j_1 - m_1)} \langle j_1\, m_1\, j_2\, -m_2 | I\, -N \rangle \times \frac{1}{\sqrt{(2J_f+1)}} \langle J_i\, M_i\, I\, N | J_f\, M_f \rangle\ S_{j_1 j_2 I}\ , \tag{13}$$

where the OBDME is identified by

$$S_{j_1 j_2 I} = \left\langle \Psi_{J_f} \left\| \left[a^\dagger_{j_2} \times \tilde{a}_{j_1} \right]^I \right\| \Psi_{J_i} \right\rangle\ . \tag{14}$$

The $0^+ \rightarrow 1^-_1;0$ (10.85 MeV) transition is a special case. The isoscalar dipole transitions correspond to compression modes of (collective) oscillations [37], and as such, there exists the possibility of spurious c.m. motion with the transition. To ensure that no such motion exists, the OBDME's obtained from the wave functions for the $1^-;0$ states must satisfy the constraint

$$\mathbf{P} = \left\langle 1^-;0 \left| \sum_{i=1}^{A} \mathbf{r}_i \right| 0^+;0 \right\rangle \equiv 0. \tag{15}$$

From the matrix element, all components of the vector $\mathbf{P}$ are also constrained to be zero and are given by

$$P_\mu = \sum_{j_1 j_2} (-1)^{j_1 + l_2 + \frac{3}{2}} \sqrt{\frac{(2j_1+1)(2j_2+1)(2l_1+1)}{12\pi}} S_{j_1 j_2 1} \langle l_1\, 0\, 1\, 0 | l_2\, 0 \rangle \begin{Bmatrix} 1 & l_1 & l_2 \\ \frac{1}{2} & j_2 & j_1 \end{Bmatrix} I_{n_2 l_2 n_1 l_1}, \tag{16}$$

where

$$I_{n_2 l_2 n_1 l_1} = \int_0^\infty r^3 dr\ R_{n_2 l_2}(r) R_{n_1 l_1}(r)\ . \tag{17}$$

Implicitly the summations include contributions from both protons and neutrons as they will in all subsequent discussion. For the OBDME's given in Table I from the present calculation, the value of the components is -1.46×10^{-3} fm. The value obtained using the OBDME's from a previous *psd* shell model calculation [10], which are also listed in Table I is 1.49 fm. The $(0+2)\hbar\omega$ and $(1+3)\hbar\omega$ wave functions are far more appropriate to describe the isoscalar dipole transition.

All form factor evaluations also require specification of the single-particle radial wave functions. In all of the calculations we have made, we have used either harmonic oscillators (for which the oscillator parameter was $b = 1.61$ fm) or Woods-Saxon wave functions (calculated using the code WSBD of Delbrouck-Habaru and Dubois [38]) for which the potential used in the Schrödinger equation has the form

$$V = V_0 \left(1 + 2\lambda [\mathbf{l} \cdot \mathbf{s}] \left(\frac{\hbar}{m_\pi c} \right)^2 \frac{1}{r} \frac{d}{dr} \right) f(r, R, a)\ , \tag{18}$$

where,

$$f(r, R, a) = \frac{1}{1 + \exp\left(\frac{r-R}{a}\right)} \tag{19}$$

with $R = r_0 A^{1/3}$. The Woods-Saxon potential parameter values we have used are listed in Table II with the calculated single particle state binding energies given in Table III. A deeper potential was used for the $0f1p$ shell to ensure that the calculations of the bound state wave functions for these shells converged. By so doing, the $0f1p$ orbits are loosely bound but then a degree of nonorthogonality is introduced. Since the single particle wave functions take the form

$$\varphi_{nlj}(\mathbf{r}) = R_{nlj}(r) \sum_{m_l m_s} \left\langle l\, m_l\, \tfrac{1}{2}\, m_s \middle| j\, m \right\rangle Y_{l m_l}(\Omega_r) \chi_{\frac{1}{2} m_s}\ , \tag{20}$$

orthogonality is guaranteed between states of different angular momenta. The question of nonorthogonality occurs with only the $0p$ and $1p$ states. With the wave

TABLE I. Proton transition density matrix elements for the $0^+ \rightarrow 1^-_1;0$ (10.85 MeV) transition. The neutron values are identical.

$j_1 : j_2$	$S_{j_1 j_2}$ [a]	$S_{j_1 j_2}$ [b]	$j_1 : j_2$	$S_{j_1 j_2}$ [a]	$S_{j_1 j_2}$ [b]
$0p_{\frac{3}{2}}:0s_{\frac{1}{2}}$	0.0102		$1p_{\frac{3}{2}}:0d_{\frac{3}{2}}$	0.0002	
$0p_{\frac{1}{2}}:0s_{\frac{1}{2}}$	0.0235		$1p_{\frac{1}{2}}:0d_{\frac{3}{2}}$	−0.0005	
$0s_{\frac{1}{2}}:0p_{\frac{3}{2}}$	0.0109	−0.0755	$0p_{\frac{3}{2}}:1s_{\frac{1}{2}}$	0.6543	1.0922
$0d_{\frac{5}{2}}:0p_{\frac{3}{2}}$	0.0014		$0p_{\frac{1}{2}}:1s_{\frac{1}{2}}$	0.3465	0.4678
$0d_{\frac{3}{2}}:0p_{\frac{3}{2}}$	0.0047		$1p_{\frac{3}{2}}:1s_{\frac{1}{2}}$	0.0038	
$1s_{\frac{1}{2}}:0p_{\frac{3}{2}}$	−0.0302		$1p_{\frac{1}{2}}:1s_{\frac{1}{2}}$	0.0022	
$0s_{\frac{1}{2}}:0p_{\frac{1}{2}}$	−0.0133	0.0941	$0d_{\frac{5}{2}}:0f_{\frac{7}{2}}$	0.0014	
$0d_{\frac{3}{2}}:0p_{\frac{1}{2}}$	−0.0012		$0d_{\frac{5}{2}}:0f_{\frac{5}{2}}$	0.00006	
$1s_{\frac{1}{2}}:0p_{\frac{1}{2}}$	0.0205		$0d_{\frac{3}{2}}:0f_{\frac{5}{2}}$	0.0002	
$0p_{\frac{3}{2}}:0d_{\frac{5}{2}}$	−0.3297	0.5534	$0s_{\frac{1}{2}}:1p_{\frac{3}{2}}$	−0.0548	
$0f_{\frac{7}{2}}:0d_{\frac{5}{2}}$	0.0002		$0d_{\frac{5}{2}}:1p_{\frac{3}{2}}$	0.0060	
$0f_{\frac{5}{2}}:0d_{\frac{5}{2}}$	0.0053		$0d_{\frac{3}{2}}:1p_{\frac{3}{2}}$	0.0020	
$1p_{\frac{3}{2}}:0d_{\frac{5}{2}}$	−0.0026		$1s_{\frac{1}{2}}:1p_{\frac{3}{2}}$	0.0005	
$0p_{\frac{3}{2}}:0d_{\frac{3}{2}}$	0.1400	−0.2111	$0s_{\frac{1}{2}}:1p_{\frac{1}{2}}$	0.0311	
$0p_{\frac{1}{2}}:0d_{\frac{3}{2}}$	−0.0934	0.1730	$0d_{\frac{3}{2}}:1p_{\frac{1}{2}}$	0.0043	
$0f_{\frac{5}{2}}:0d_{\frac{3}{2}}$	−0.0006		$1s_{\frac{1}{2}}:1p_{\frac{1}{2}}$	−0.0009	

[a] $(0+2)\hbar\omega$.
[b] *psd* shell model [10].

TABLE II. Woods-Saxon parameters used for the single particle states in ^{12}C.

	V_0 (MeV)	r_0 (fm)	a_0 (fm)	λ
$0s \rightarrow (1s0d)$	−62.5	1.35	0.65	7.0
$0f1p$	−90.0	1.35	0.65	0.0

TABLE III. Binding energies for the single particle states in ^{12}C as calculated from the Woods-Saxon potentials in Table II.

	State	E_B (MeV)		State	E_B (MeV)
1	$0s_{\frac{1}{2}}$	−38.75	6	$1s_{\frac{1}{2}}$	−5.87
2	$0p_{\frac{3}{2}}$	−22.37	7	$0f_{\frac{7}{2}}$	−1.04
3	$0p_{\frac{1}{2}}$	−20.65	8	$0f_{\frac{5}{2}}$	−1.07
4	$0d_{\frac{5}{2}}$	−6.28	9	$1p_{\frac{3}{2}}$	−3.53
5	$0d_{\frac{3}{2}}$	−3.58	10	$1p_{\frac{1}{2}}$	−3.53

functions we have used, the volume integrated overlap between the $0p$ and $1p$ radial wave functions is zero to within 1 part in 10^{-3}.

The elastic electron scattering form factors for ^{12}C are presented in Fig. 4, in which the data shown are those of Jansen *et al.* [39] (squares), Sick and McCarthy [40] (diamonds), and Nakada *et al.* [41] (circles). Both the $(0+2)\hbar\omega$ and the $0p$-shell model wave functions have been used in the calculations of the form factors; the results displayed being the solid and dashed lines, respectively. There is excellent agreement with data irrespective of whichever model and whichever set of single particle wave function are used, indicating that the sets of single particle wave functions used are appropriate for use in analyses of inelastic scattering data with both the $0p$ and multi-$\hbar\omega$ shell model wave functions. However the structure aspects of importance for elastic scattering are just the (ground state) single particle state occupancies, and they are so dominated by the $0p$-shell attributes in all prescriptions for the ground state that large basis space effects are not tested. Inelastic transitions are required for that.

The inelastic longitudinal and transverse electron scattering form factors for the transition to the $2_1^+;0$ (4.44 MeV) state in ^{12}C are displayed in Fig. 5. Therein, the data for the longitudinal form factor of Flanz *et al.*

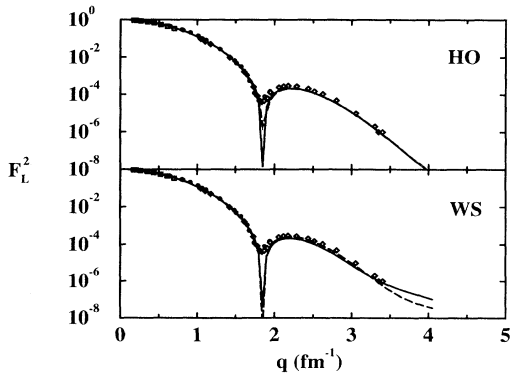

FIG. 4. Elastic electron scattering for factor for ^{12}C, calculated using the $(0+2)\hbar\omega$ wave functions (solid line) and the Cohen and Kurath $0p$-shell model wave functions (dashed line). Harmonic oscillator (HO) and Woods-Saxon (WS) single particle wave functions were used. The data are those of Jansen *et al.* [39] (squares), Sick and McCarthy [40] (diamonds), and Nakada *et al.* [41] (circles).

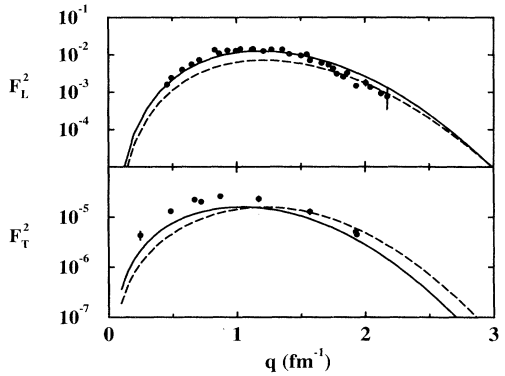

FIG. 5. Longitudinal (F_L^2) and transverse (F_T^2) electron scattering form factors to the $2_1^+;0$ (4.44 MeV) state in ^{12}C. The data are those of Flanz *et al.* [42]. Calculations are those using the $(0+2)\hbar\omega$ wave functions (solid line) and Cohen and Kurath $0p$-shell model wave functions (dashed lines).

[42] are compared in the top segment of this figure with the results of our calculations using the $(0+2)\hbar\omega$ (solid line) and the $0p$-shell (dashed line) model wave functions. Both calculations were made using the harmonic oscillator single particle wave functions. The results of our calculations made using the Woods-Saxon wave functions are so similar that they are not displayed. The $0p$-shell model calculation underestimates the data by a factor of 2. Using the $(0+2)\hbar\omega$ wave functions gives far better agreement with the data; the additional transitions obtained by the inclusion of the $2\hbar\omega$ components in the wave functions provide the necessary extra strength to give agreement with the data. The result of the $(0+2)\hbar\omega$ calculation is equivalent to that obtained recently by using the symplectic collective model [43].

The situation is similar in the case of the transverse electric electron scattering form factor from the excitation of the $2_1^+;0$ (4.44 MeV) state. The results are displayed in the bottom segment of Fig. 5. Therein the data of Flanz *et al.* [42] are compared to the results of our calculations made using the $(0+2)\hbar\omega$ (solid line) and $0p$-shell (dashed line) model structures. In each case, the calculation fails to reproduce the magnitude of the data. However, the q dependence of the form factor calculated using the $(0+2)\hbar\omega$ wave functions almost exactly agrees with that of the data as, with an enhancement of 1.6, the result reproduces the data very well.

The longitudinal form factors for the excitation of the $3_1^-;0$ (9.64 MeV) and $1_1^-;0$ (10.85 MeV) states in ^{12}C are displayed in Fig. 6 as sections (a) and (b), respectively. Therein the results found using the $(1+3)\hbar\omega$ wave functions are displayed by the solid curves while the dashed curves represent the results obtained using the PHM spectroscopy. Both sets of calculations used Woods-Saxon single nucleon wave functions. In Fig. 6(a) and (b) the results of our calculations are compared with the data of Crannell [44] and of Torizuka *et al.* [45], respectively. For both form factors, the $(1+3)\hbar\omega$ wave functions give the better agreement with the data, notably for the lower momentum transfer regime. In par-

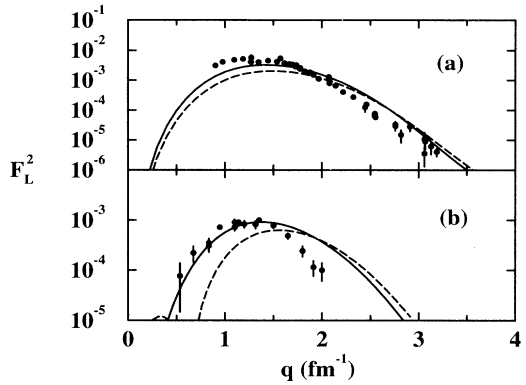

FIG. 6. The longitudinal form factors for the excitation of the $3_1^-;0$ (9.64 MeV) state (a) and of the $1_1^-;0$ (10.85 MeV) state (b) in ^{12}C. The data are those of Crannell [44] and of Torizuka *et al.* [45] for the 3^- and 1^- excitations, respectively. The results of calculations made using the $(1+3)\hbar\omega$ and PHM model wave functions are displayed by the solid and dashed lines, respectively.

ticular we reproduce the magnitudes of the data so that there is no need for any scale enhancement one could associate with core polarization.

The transverse electric form factor for the $0^+ \rightarrow 2_1^+;1$ (16.11 MeV) transition is displayed in Fig. 7, wherein the data of Flanz *et al.* [42] are compared with the results of our calculations made using the $(0+2)\hbar\omega$ (solid line) and the $0p$-shell model (dashed line) wave functions. Clearly, the $(0+2)\hbar\omega$ calculation is in better agreement with the data. The effect of the enlarged basis for this isovector transition has been to reduce the net transition strength. This occurs because the higher shell entries in the OBDME's are formed at the expense of the strength of the dominant shell transition values in this case.

A similar reduction in transition strength is observed with the isoscalar magnetic dipole form factors, but that is caused by an increased destructive interference between proton and neutron contributions. Further there is some evidence for isospin mixing between the $1_1^+;0$ (12.71 MeV) and $1_1^+;1$ (15.11 MeV) states [46]. The transverse $M1$ electron scattering form factors for these states are displayed in Fig. 8. Therein, the data of Flanz *et al.* [46] are compared with the results of our calculations made using the $(0+2)\hbar\omega$ (solid line) and the CK (dashed line) wave functions. The contributions from meson exchange currents have been neglected in these studies, but as they are isovector in nature, they should affect only the high-q part of the isovector transverse form factor. Such is evident in the calculations of Flanz *et al.* [46]. Meson exchange current effects do not account for the disparity between calculated and measured isoscalar $M1$ form factors at low momentum transfer. For that isospin mixing between the two states is required. We assume that to have the form

$$\begin{bmatrix} 12.71 \\ 15.11 \end{bmatrix} = \begin{bmatrix} \alpha & \beta \\ -\beta & \alpha \end{bmatrix} \begin{bmatrix} T=0 \\ T=1 \end{bmatrix}, \tag{21}$$

where $\beta = 0.07$ [46] and $\alpha = \sqrt{1-\beta^2} = 0.9975$. The results of form factor calculations made incorporating this mixing are portrayed by the dot-dashed lines in Fig. 8. As is evident, there is a significant improvement in the prediction of the isoscalar form factor but there is very little change in the isovector form factor caused by this mixing. The results are consistent with the findings of Flanz *et al.* [46]. The reason for this improvement is illustrated in Fig. 9, in which the individual proton and neutron contributions to the isoscalar form factor are shown by the dot-dashed and dashed lines, respectively. The total isoscalar transverse form factor is the result of the serious destructive interference between the proton and neutron amplitudes. Hence the small changes to the transition densities introduced by the isospin mixing suffices to make a large change in the final total form factor. The proton-neutron interference is constructive in the case of the isovector transition so that there is very little effect on the predicted isovector transverse magnetic form factor.

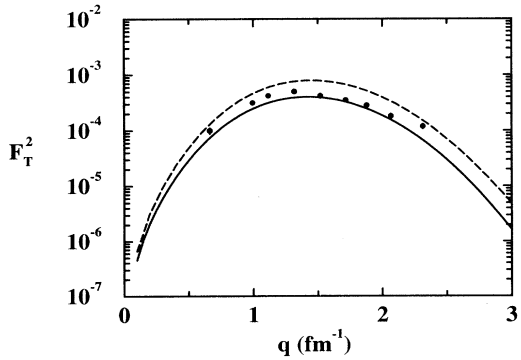

FIG. 7. Transverse electron scattering form factor to the $2_1^+;1$ (16.11 MeV) state in ^{12}C. The data of Flanz *et al.* [42] are compared to the calculation using the $(0+2)\hbar\omega$ wave functions (solid line) and the $0\hbar\omega$ wave functions (dashed line).

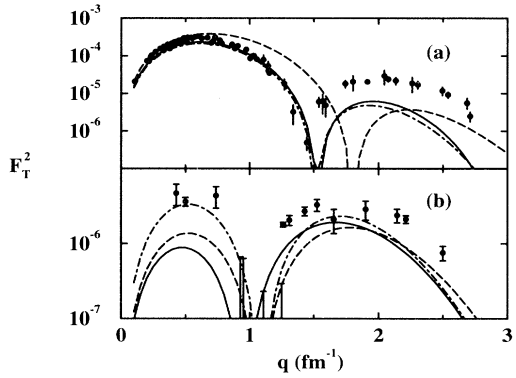

FIG. 8. Transverse $M1$ electron scattering form factors to (a) the $1_1^+;1$ (15.11 MeV) state and (b) the $1_1^+;0$ (12.71 MeV) state in ^{12}C. The data of Flanz *et al.* [46] are compared to the calculation using the $(0+2)\hbar\omega$ wave functions (solid line) and the Cohen and Kurath wave functions (dashed line). The dot-dashed line is the result of assuming the two-level isospin mixing as described in the text.

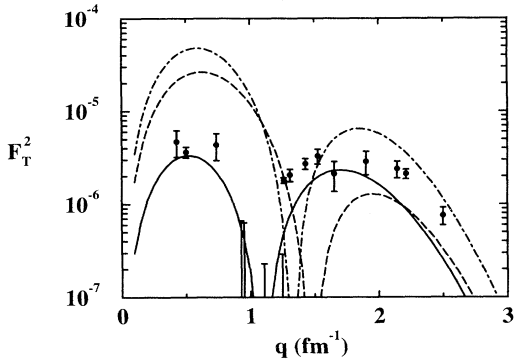

FIG. 9. Proton contribution (dot-dashed line) and neutron contribution (dashed line) to the transverse $M1$ form factor for scattering to the $1_1^+;0$ (12.71 MeV) state. The total form factor is given by the solid line.

The longitudinal form factor for the $0^+ \rightarrow 4_1^+;0$ (14.08 MeV) transition is displayed in Fig. 10. The $0p$-shell model cannot predict any state with $J > 3$. Hence, the data of Nakada *et al.* [41] are compared with the results of calculations made using the $(0+2)\hbar\omega$ and the projected Hartree-Fock (PHF) models [47] of spectroscopy. The latter gives a form factor in close agreement with the data while the $(0+2)\hbar\omega$ calculation underestimates the data by a factor of three. The close agreement with data from the PHF calculation indicates that $> 2\hbar\omega$ components are required in the wave function. Two results are shown for each spectroscopic model used. The small dashed and dash-dotted curves were obtained by using harmonic oscillator functions while those portrayed with the solid and long dashed curves used Woods-Saxon functions. The differences caused by our choice of single particle wave functions are not large and occur at higher momentum transfers where higher order scattering processes may be needed in any calculation to use the results

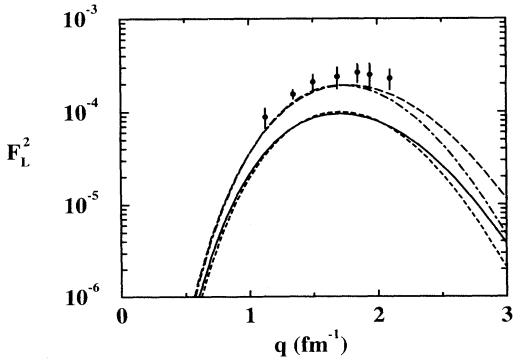

FIG. 10. Longitudinal $E4$ electron scattering form factor for the $0^+ \rightarrow 4_1^+;0$ (14.08 MeV) transition in ^{12}C. The data of Nakada *et al.* [41] are compared to the calculation using the $(0+2)\hbar\omega$ wave functions (solid line with Woods-Saxon wave functions and short-dashed line with harmonic oscillators) and that using the PHF wave functions [36,47] (long-dashed line with Woods-Saxon wave functions and dot-dashed line with harmonic oscillators).

confidently to select one wave function form as the more appropriate.

IV. ANALYSIS OF ELASTIC PROTON SCATTERING DATA

The cross sections and analyzing powers for 200 MeV protons elastically scattered from ^{12}C have been calculated by using the DWBA91 code. That coordinate space code requires as input, the single nucleon shell occupancies of the target state, the single particle bound state wave functions, and the effective NN interaction. The single particle occupancies for the case of ^{12}C have been obtained from the spectroscopic models described in the previous section. The large basis effects are not very significant in so far as the occupancies are concerned. The effective interaction required is of the form we have discussed previously, i.e., $g_{\rm eff}^{(i)ST}(|\mathbf{r}|;E,k_f(r))$, and it is folded with the nuclear structure functions allowing explicitly for the antisymmetrization of the projectile and each and every target nucleon. Further, a kinematic correction to the effective NN interaction is required to describe a given NA system. In accordance with Eq. (19) in Ref. [6], this scaling factor for the case of 200 MeV protons on ^{12}C is 0.93725. It remains then only to determine the specific radial variation of the Fermi momentum which is defined by

$$k_f(r) = \left(\frac{3\pi^2}{2}\rho(r)\right)^{\frac{1}{3}} . \tag{22}$$

The density profile we have chosen to be the three parameter Fermi distribution

$$\rho(r) = \frac{\rho_0(1+wr^2/c^2)}{(1+e^{(r-c)/z})} , \tag{23}$$

with $\rho_0 = 0.182$ nucleons/fm^3, $c = 2.355$ fm, $z = 0.5224$ fm, and $w = -0.149$ [48].

We will identify by the label "DD" all results obtained from complete calculations of elastic scattering, i.e., those made using the nonlocal optical potential microscopically generated with the medium modified effective interaction. The same label will be used in our later discussion of inelastic scattering calculations. Also we have used an effective interaction defined by mapping the free NN t matrices and results obtained with the nonlocal optical potential found thereby are identified as the "free" ones hereafter. Note that this corresponds to the choice $k_f(r) = 0$ for all radii.

The forms of the optical potentials specified in DWBA91 follow from identification of the net effective interaction between the projectile and each and every nucleon in the target as

$$V_{\rm eff}(|\mathbf{r}|;E,k_f) = \sum_{LST}(2L+1)\, V_L^{ST}(r_1,r_2;E,k_f)\, P_L(\cos\theta)\, P^S P^T, \tag{24}$$

where $|\mathbf{r}| = |\mathbf{r}_1 - \mathbf{r}_2|$ and $V_L^{ST}(r_1, r_2; E, k_f)$ are two body spin (S) and isospin (T) multipoles. Those multipoles are related to the effective interaction by a series of Fourier and Bessel transformations [49], viz.,

$$V_L^{ST}(r_1, r_2; E, k_f) = \frac{2}{\pi} \int W^{ST}(q; E, k_f)\; j_L(qr_1)\; j_L(qr_2)\; q^2\; dq, \qquad (25)$$

where

$$W^{ST}(q; E, k_f) = \sum_i \int e^{(i\mathbf{q}\cdot\mathbf{r})}\; g_{\text{eff}}^{(i)ST}(|\mathbf{r}|; E, k_f(r))d\mathbf{r}\ . \qquad (26)$$

Antisymmetrizing the NA wave function leads to a nonlocal optical potential. This takes the form

$$\begin{aligned} U(\mathbf{r}_1, \mathbf{r}_2; E) &= \delta(\mathbf{r}_1 - \mathbf{r}_2) \sum_n \zeta_n \int \varphi_n^*(\mathbf{s})\; v^D\{\mathbf{r}_{1s}, E; \rho[k_f(s)]\}\; \varphi_n(\mathbf{s})\; d\mathbf{s} \\ &\quad + \sum_n \zeta_n \varphi_n^*(\mathbf{r}_1)\; v^{Ex}\{\mathbf{r}_{12}, E; \rho[k_f(r_2)]\}\; \varphi_n(\mathbf{r}_2) \\ &\Rightarrow U_D(\mathbf{r}_1; E) + U_{Ex}(\mathbf{r}_1, \mathbf{r}_2; E)\ , \end{aligned} \qquad (27)$$

upon folding the effective interaction, Eq. (24), with the density matrix elements of a nucleus. Here v^D and v^{Ex} are appropriate combinations [4,49] of the ST channel elements of the effective interaction of Eq. (24), $\varphi_j(\mathbf{r})$ are the single (bound) nucleon wave functions and ζ_n are the shell occupancies in the target state.

The leading term, the "direct" term has been used in the past as the sole contributing element. It equates to the interaction one would specify by the so-called $t\rho$ approximation. At 200 MeV, it is inappropriate to use such a microscopic direct potential solely in an analysis of scattering data since the nonlocality (due to the antisymmetrization contributions to the optical potential) cannot be ignored and also the choice to use the t rather than the g matrices makes a considerable difference. In Fig. 11, the direct potentials calculated by the prescription we have set down, are shown for the effective interaction with profiles, Eq. (23), limited to different maximum densities. The real and imaginary parts of the central and spin-orbit components of the direct potentials that result from the folding process are displayed for the free and complete (DD) cases by the long dashed and solid curves, respectively. The dot-dashed and small dashed curves show the "direct" potentials that result if one uses medium modified g matrices and a density profile limited to $\frac{1}{3}$ and $\frac{2}{3}$ of the nuclear central density, respectively. In those two cases, for radii at which the nuclear density would normally exceed the limits, the limit form of the g matrices were used. The "direct" spin-orbit interaction is quite weak and essentially real with little variation due to medium effects upon the g matrix specification. However, there is a clear progressive and marked enhancement of the calculated (central local real) optical potential strength as one moves from using free to complete density dependent forces. Likewise the imaginary part of the central interaction changes from strongly productive to weakly absorptive with gradual inclusion of the medium modifications. This suggests that one cannot expect a calculation made using a free NN interaction with a $t\rho$ approach leading to a local NA optical potential, to describe adequately elastic scattering data. Without the exact nonlocal components, arbitrary adjustments to the effective t matrices and/or use of an equivalent local approximation to the true exchange terms, must be made. Such make the analyses nucleus and transition dependent.

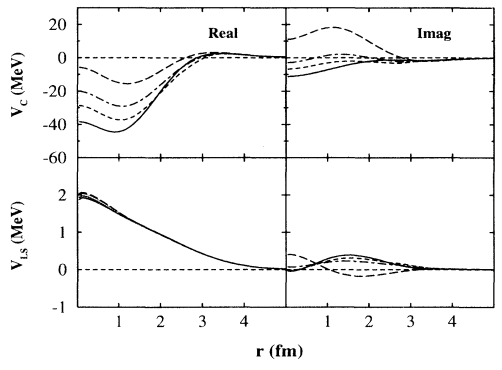

FIG. 11. The "direct" components of the calculated microscopic optical potentials found by folding the free effective and the complete, density dependent, effective interactions with the density matrices of the ground state of ^{12}C and displayed by the long dashed and solid curves, respectively. With the medium modifications limited to $\frac{1}{3}$ and $\frac{2}{3}$ central nuclear density, the results shown by the dot-dashed and small dashed curves, respectively, result.

The cross sections and analyzing powers that result in using our calculated optical potentials are compared with data [2] in Figs. 12 and 13. Those calculations were made using the ground state occupancies given by the $(0+2)\hbar\omega$ shell model calculation. Consistent with the results found with the elastic electron scattering form factors, Fig. 4, using the CK structure values makes virtually no change to the proton elastic scattering predictions from those displayed. In Fig. 12 the solid and dashed curves display the results obtained by using Woods-Saxon and harmonic oscillator bound state wave functions, respectively, for the orbitals in Eq. (27) and the "free" and DD results are shown in the left- and right-side panels. It is evident

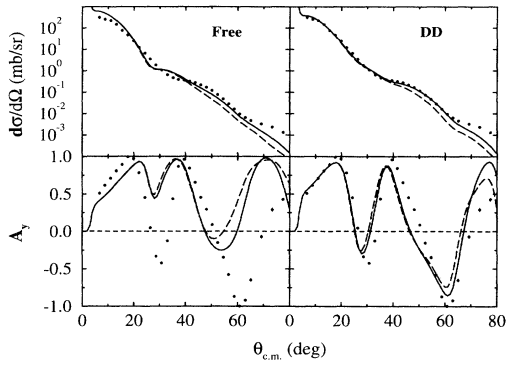

FIG. 12. The 200 MeV proton elastic scattering cross section and analyzing power data [2] compared with the results found using the (nonlocal) microscopic optical potentials built using the free NN t matrices (left) and the full interaction (right). The solid and dashed curves display the results found using Woods-Saxon and harmonic oscillator single particle bound state functions, respectively, in the calculations.

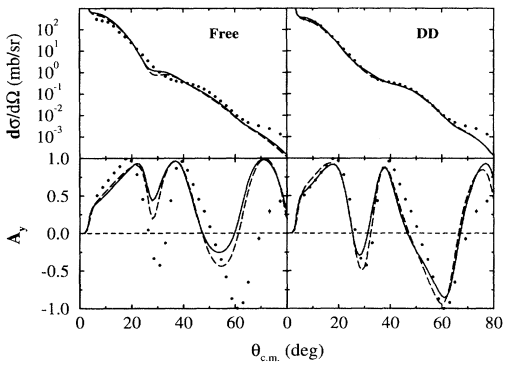

FIG. 13. The 200 MeV proton elastic scattering data [2] compared with the results found using the microscopically calculated optical potentials built upon free and density dependent effective interactions. The solid and dashed curves give the results found when the Paris [18] and BonnB [25] NN forces were used to specify the input t matrix information, respectively.

the density dependent, Woods-Saxon bound state result matches the cross-section data best. That is even more obvious with the analyzing power. The DD results are far better in agreement with observation than the "free" ones.

In Fig. 13 the "free" and DD cross sections and analyzing powers are shown from optical potentials calculated using the Paris and BonnB interactions as the basic input NN interactions. The Paris and BonnB results are shown by the solid and dashed curves, respectively. Again the density dependent results, whether obtained from the Paris or BonnB input, are in far better agreement with the data, and especially the analyzing power. There is little to choose between the results found with the two differing "realistic" starting interactions, however, and such is also the case with all of the inelastic scattering cases studied and discussed next.

V. ANALYSES OF INELASTIC PROTON SCATTERING DATA

The theoretical derivation of the scattering amplitudes in the DWA for inelastic scattering from nuclei have been presented in detail elsewhere [50] and so only the salient features are given herein. With $\mathcal{A}_{01}$ being the two nucleon antisymmetrization operator, the DWA transition amplitudes can be written as

$$T^{M_f M_i \nu' \nu}_{J_f J_i}(\theta) = \left\langle \chi^{(-)}_{\nu'}(\mathbf{k}_o 0) \right| \left\langle \Psi_{J_f M_f}(1\cdots A)\right| \times A\mathbf{g}_{\rm eff}(0,1) \times \mathcal{A}_{01}\left\{ \left|\chi^{(+)}_{\nu}(\mathbf{k}_i 0)\right\rangle |\Psi_{J_i M_i}(1\cdots A)\rangle \right\} , \tag{28}$$

wherein the distorted wave functions are denoted by $\chi^{(\pm)}_{\mu}(\mathbf{k}q)$ for an (incoming/outgoing) proton with spin projection μ, wave vector $\mathbf{k}$, and coordinate set "q." The radial (partial wave) components of these are generated from the microscopic optical model calculations that were discussed previously. The A-nucleon nuclear structure wave functions are denoted by $\Psi_{JM}(1\cdots A)$ and since all pairwise interactions between the projectile and every target nucleon is taken to be the same, it is convenient to make a cofactor expansion of each, viz., to use

$$|\Psi_{JM}(1\cdots A)\rangle = \frac{1}{\sqrt{A}} \sum_{j,m} |\varphi_{jm}(1)\rangle\, a_{jm}\, |\Psi_{JM}(1\cdots A)\rangle \ . \tag{29}$$

Therewith all dependences upon the coordinate "1" selected to be the active entry in the "$\mathbf{g}_{\rm eff}$" can be isolated so that the transition amplitudes expand to the form

$$T^{M_f M_i \nu' \nu}_{J_f J_i}(\theta) = \sum_{j_1,j_2,m_1,m_2} \left\langle \Psi_{J_f M_f} \left| a^{\dagger}_{j_2 m_2} a_{j_1 m_1} \right| \Psi_{J_i M_i} \right\rangle \left\langle \chi^{(-)}_{\nu'}(\mathbf{k}_o 0)\right| \langle \varphi_{j_2 m_2}(1)|\ \mathbf{g}_{\rm eff}(0,1) \times \mathcal{A}_{01}\left\{ \left|\chi^{(+)}_{\nu}(\mathbf{k}_i 0)\right\rangle |\varphi_{j_1 m_1}(1)\rangle \right\} . \tag{30}$$

To use the Wigner-Eckart theorem the product of creation and annihilation operators must be expressed in terms of elements of an irreducible tensor operator and that is as specified in Eq. (12). Then the scattering amplitudes become

$$T^{M_f M_i \nu' \nu}_{J_f J_i}(\theta) = \sum_{j_1, j_2, I(N)} \frac{1}{\sqrt{2J_f+1}} \langle J_i\, M_i\, I\, N | J_f\, M_f \rangle\ S_{j_1 j_2 I} \sum_{m_1, m_2} (-1)^{(j_1 - m_1)} \langle j_1\, m_1\, j_2\, -m_2 | I\, -N \rangle$$
$$\times \left\langle \chi^{(-)}_{\nu'}(\mathbf{k}_o 0) \right| \langle \varphi_{j_2 m_2}(1) |\ \mathbf{g}_{\rm eff}(0,1)\ \mathcal{A}_{01} \left\{ \left| \chi^{(+)}_{\nu}(\mathbf{k}_i 0) \right\rangle\ |\varphi_{j_1 m_1}(1)\rangle \right\}\ , \tag{31}$$

wherein the $S_{j_1 j_2 I}$ are the OBDME's defined by Eq. (14). They are exactly those quantities required from the nuclear structure calculations to give the electron scattering form factors discussed previously.

DWA calculations of diverse inelastic scattering cross sections and analyzing powers from the scattering of 200 MeV protons from ^{12}C are compared with data in the next set of figures. In those figures the results shown in the left-hand panels were obtained using an effective interaction based solely upon the free Paris t matrices. Those in the right-hand panels were found by using the full medium modified g matrices to define the effective transition operator. With one exception, the results for positive parity transitions displayed by the dashed curves were obtained using the CK wave functions while those displayed by the solid curve were calculated using our $(0+2)\hbar\omega$ structure. The exception is for the $4^+_1;0$ (14.08 MeV) excitation wherein the dashed curves will display the results found by using spectroscopic amplitudes from an axially symmetric PHF calculation [36]. The CK model, being a purely $0p$-shell study, does not support any sensible prescription for the $4^+_1;0$ state. With the negative parity excitations, the dashed curves are the results of DWA calculations made using the spectroscopy of the PHM scheme [28]. In all cases the distorted waves were generated using the optical potential found by folding the same effective interaction used as the inelastic scattering transition operator with the occupation numbers for the ground and relevant excited states of ^{12}C. Thus the effective NN interaction specifies both the (nonlocal) optical potentials used to define the distorted wave functions and the inelastic scattering transition operator in the two particle fully antisymmetrized matrix elements specified in Eq. (31).

The results of our DWA calculations for the cross section and analyzing power from 200 MeV protons exciting the $2^+_1;0$ (4.44 MeV) state in ^{12}C are compared with the data in Fig. 14. With both the free and density dependent effective interactions, the larger based structure calculations increase the predicted magnitudes above those given with the CK wave functions into quite good agreement with the data. The results reflect the similar effects observed when those wave functions were used in the calculation of the electron scattering form factors in Sec. III B. The density dependent effective interaction gives cross sections in best agreement with the data reproducing the shoulder effect in the $20-40°$ region in particular. The analyzing power results are not as good fits to the measured values. They do reflect the general shape of the data however, and the density dependent results more so than the free ones in the scattering angles to 50°. With this transition the central and two body spin-orbit attributes of the transition operator are the most important contributing features. We stress that there has been no core polarization correction applied to the calculated cross-section magnitudes shown in Fig. 14, nor indeed of any that we show hereafter, and as was the case with all of the electron scattering form factors displayed previously. But in other studies [10] that was not the case. The cross-section results they displayed were scaled to give the best fit to the data. The justification for so doing was that core polarization corrections are needed when, as they did, the CK shell model of structure was used to describe the nuclear transitions. But those scalings were not consistent with the enhancement the same structure model needs to match electron scattering form factors and/or γ-decay rates.

The results of our DWA calculations of 200 MeV proton inelastic scattering to the $3^-_1;0$ (9.64 MeV) state are shown in Fig. 15. The free and density dependent effective interaction results are quite similar and are in good agreement with the data. As this final state cannot be specified by the CK model, the $(1+3)\hbar\omega$ shell model results (solid curves) are compared with those obtained by using the PHM [28] prescription. A similar result is found with the scattering to the $1^-_1;0$ (10.85 MeV) state; albeit in this case the free effective interaction cross sections are marginally better in agreement with the data given the two spectroscopies used. But the analyzing power is better reproduced by the DD calculation. Those results are displayed in Fig. 16. Consistent with the results found from our analyses of the electron scattering form factors, no enhancement of the $(1+3)\hbar\omega$ OBDME's is needed to

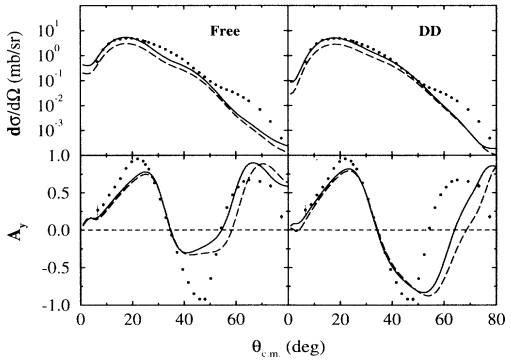

FIG. 14. The differential cross section and analyzing power from the inelastic scattering of 200 MeV protons from ^{12}C leading to the $2^+_1;0$ (4.44 MeV) state. The data [2] are compared with the results of our DWA calculations made using the microscopic optical model interactions for the free and density dependent interactions (left and right panels) and the $(0+2)\hbar\omega$ and CK ($0p$) models of spectroscopy (solid and dashed curves).

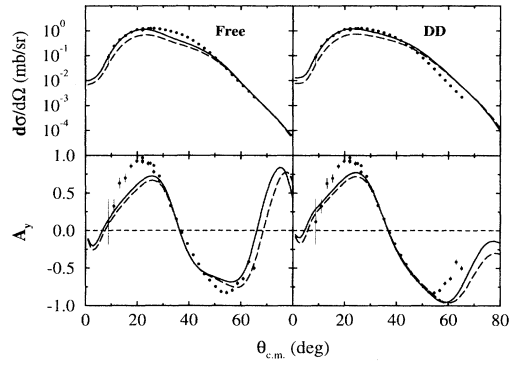

FIG. 15. The inelastic (200 MeV) proton scattering data [2] from the excitation of the $3_1^-;0$ (9.64 MeV) state in ^{12}C compared with the results of DWA calculations made using the free and density dependent effective interactions (left and right, respectively) and with the $(1+3)\hbar\omega$ and PHM spectroscopy (solid and dashed curves, respectively).

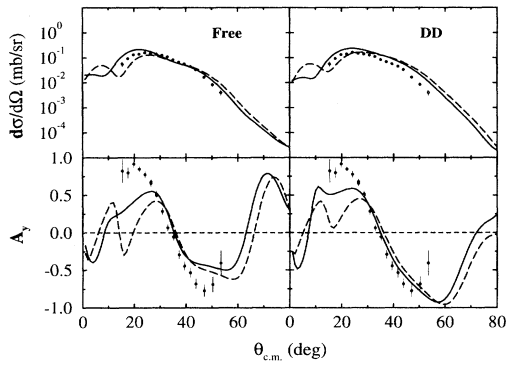

FIG. 16. As for Fig. 15 but for the excitation of the $1_1^-;0$ (10.84 MeV) state.

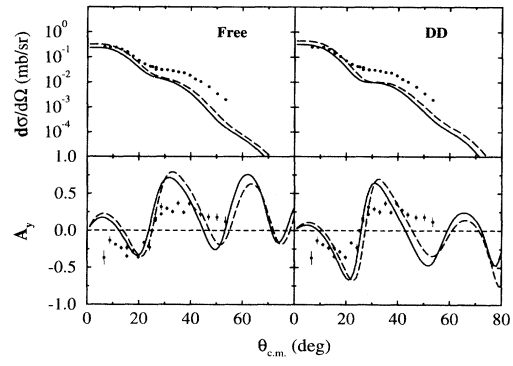

FIG. 17. As for Fig. 14 but for the excitation of the $1_1^+;0$ (12.72 MeV) state.

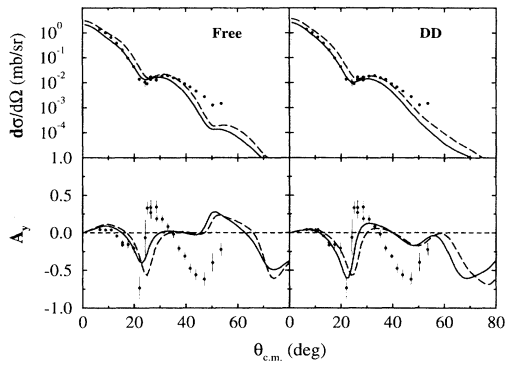

FIG. 18. As for Fig. 14 but for the excitation of the $1_1^+;1$ (15.11 MeV) state.

give the magnitudes of these cross sections.

The magnetic dipole excitations are shown in Figs. 17 and 18 for the isoscalar (12.71 MeV) and isovector (15.11 MeV) transitions, respectively. Strength suppression with bigger basis spectroscopy is evident from these calculations, again concurring with the results found for the electron scattering form factors. The density dependent, large basis spectroscopy calculation results are marginally the best of the set. None give the magnitude of the larger scattering angle measured cross section however, and the analyzing power is less structured than predicted. The isovector dipole transition cross section is well reproduced by our favored, density dependent large basis spectroscopy model but now the measured analyzing power data have severe variations with momentum transfer which have not been reproduced by the calculations. Unlike the case of the electron scattering form factor, isospin mixing does not account for these variations as the effective NN interactions are charge independent. Finally we note that, while the tensor force component of the transition operator are important elements in the calculations of both the isoscalar and isovector excitations, the spin-orbit terms are essential for the isoscalar scattering amplitudes but it is the central terms that are so for the isovector ones.

The $2_1^+;1$ (16.11 MeV) excitation results are shown in Fig. 19. The diminution of transition strength ex-

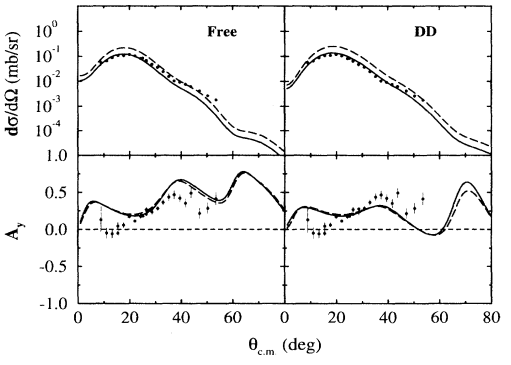

FIG. 19. As for Fig. 14 but for the excitation of the $2_1^+;1$ (16.11 MeV) state.

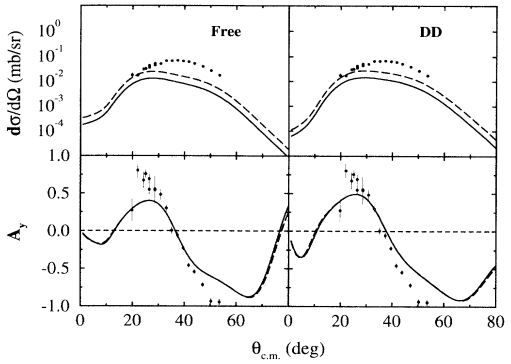

FIG. 20. The differential cross section and analyzing power from inelastic (200 MeV) proton scattering to the $4_1^+;0$ (14.08 MeV) state in ^{12}C. The solid and dashed curves show DWA results found using the $(0+2)\hbar\omega$ and PHF models of structure.

pected with larger basis calculations of such transitions is observed with both the free and density dependent $(0+2)\hbar\omega$ structure calculations giving very good agreement with the data. The reduction of the cross-section predictions with the larger basis spectroscopy matches that noted with the transverse form factor from electron excitation of this state. In this case, all attributes of the transition operator are important in the calculations, and again we stress that no core polarization corrections have been used to give good agreement with the data.

The results of our DWA calculations for the cross section and analyzing power from 200 MeV protons exciting the $4_1^+;0$ (14.08 MeV) state in ^{12}C are compared with the data in Fig. 20. As with other normal parity transitions, the central and two body spin-orbit attributes of the transition operator are the most important contributing features. In this case, as with the electron scattering form factor calculations shown in Fig. 10, the dashed curves give the results obtained using the PHF model spectroscopic amplitudes [36]. The PHF model yields a larger cross section than does the $(0+2)\hbar\omega$ model and while both results reflect the general shape of the data neither gives the correct magnitude for the cross section. That was not so with the longitudinal electron scattering form factors from which we surmised that the inherent larger basis aspect of the PHF structure was essentially the needed improvement to the $(0+2)\hbar\omega$ shell model. With proton inelastic scattering then one may surmise that the scattering process is incomplete, with perhaps some channel coupling effects now being evident. But only with even larger basis structure calculations can one hope to do more than surmise.

VI. CONCLUSIONS

Elastic and inelastic scattering data, cross sections, and analyzing powers, from the scattering of 200 MeV protons off ^{12}C have been analyzed using a completely microscopic model of the reactions. The nuclear structure required for those analyses was obtained from large basis shell model calculations and comparisons of that structure have been made with the spectral properties of the standard (CK) small basis structure of ^{12}C and with those of large basis projected Hartree-Fock calculations. All established spin-parity assignments to 20 MeV excitation in ^{12}C are matched by our calculated spectrum with most states being in good agreement. We have analyzed electron scattering form factors from excitation of most states in the low-lying spectrum as they are sensitive to the same OBDME's required in analyses of proton inelastic scattering using the microscopic DWA model. The results have shown that the structure so defined is very good, and in addition, we have seen evidence of the degree of isospin mixing one should consider with the 1^+ states. With the large basis space structure, the electron scattering form factors indicate that no enhancement, such as core polarization corrections are required for most transitions. Also the single particle wave functions were not changed with any transition analysis and good to excellent results so far as the momentum transfer variations are concerned have been found. Woods-Saxon functions are the preferred set.

A fully microscopic calculation of proton scattering from ^{12}C next requires the effective NN interaction within the nuclear medium be specified. This we have done in the form that can be used in the scattering analysis program of Raynal, DWBA91. The effective interaction then has central, tensor, and two-body spin-orbit attributes each with a sum of Yukawa functions (in coordinate space) as the form factor, and with each form factor varied according to the location of the interaction within the nuclear medium. We selected the ranges and strengths of those form factor components by optimizing the half-off-shell t and g matrix elements they give in infinite nuclear matter of diverse densities against those of the Paris NN interaction. We have placed particular emphasis upon the match between the sets of elements around the on-shell momentum (1.55 fm^{-1}) for all low J NN channels.

To analyze elastic scattering data, the optical potential must be specified by folding the effective NN interaction with the density matrix elements of the ground state of ^{12}C. That requires the occupation numbers of bound nucleons in ^{12}C and they differ little between the various models of structure. But the results are very nonlocal and quite sensitive to the medium modifications that distinguish the effective interaction from the free NN counterpart. With Woods-Saxon bound state wave functions, full treatment of the nonlocal character of the optical potential gave extremely good agreement with the measured cross section and analyzing power up to $\sim 60°$ in the c.m. scattering angle.

The same microscopic optical potential, and the relevant one for each and every final state of a (p,p') reaction, have been used to define the distorted wave functions for DWA calculations of inelastic scattering cross sections and analyzing powers. The same effective interaction was used as the NN transition operator in those evaluations. With our large basis model of nuclear structure giving the OBDME's, fits to the measured data at 200 MeV range from quite good to excellent. Details of some transitions remain unresolved, but the results are

as good or better than have been found in equivalent studies in the past. Notably the results for the analyzing powers are good. But the data from the so-called strongly collective states, the $2_1^+;0$ and $3_1^-;0$ excitations, are well reproduced by our calculations and without need for any core polarization corrections to give the observed magnitudes. The same is true for the excitations of the $1_1^+;1$ and $2_1^+;1$ states. The data from other transitions are not as well reproduced but the results are quite good nevertheless.

In summary, we have presented a new effective NN interaction for use in elastic and inelastic proton scattering analyses and a new large space calculation of the needed structure in such analyses. With those, the optical potential has been calculated fully microscopically and its nonlocality retained in the Schrödinger equation. The result for the elastic scattering of 200 MeV protons from ^{12}C is excellent. The fully microscopic DWA was then used to evaluate cross sections and analyzing powers for inelastic scattering off ^{12}C with very good results. No adjustments have been made to the effective interactions specifications or to the structure input with any transition and none are needed in some.

ACKNOWLEDGMENTS

The financial support of the Australian Research Council (ARC) is gratefully acknowledged as is the hospitality of the staff and students of the School of Physics in the University of Melbourne shown to R. de S. during a visit sponsored in part by the ARC. We also thank Professor J. Raynal for the use of his code DWBA91 and for a number of very useful communications with regard to its operation.

[1] P. E. Hodgson, *The Nucleon Optical Potential* (World Scientific, Singapore, 1994).
[2] J. R. Comfort, G. L. Moake, C. C. Foster, P. Schwandt, and W. G. Love, Phys. Rev. C **26**, 1800 (1982); P. Schwandt, private communication.
[3] L. Ray, Phys. Rev. C **41**, 2816 (1990); J. J. Kelly and S. J. Wallace, *ibid.* **49**, 1315 (1994).
[4] H. V. von Geramb and K. Nakano, in *The Interaction Between Medium Energy Nucleons and Nuclei*, AIP Conf. Proc. 97, edited by H. O. Meyer (AIP, New York, 1982), p. 44; L. Rikus, K. Nakano, and H. V. von Geramb, Nucl. Phys. **A414**, 413 (1984).
[5] A. Ingermarsson, O. Jonsson, and A. Hallgren, Nucl. Phys. **A319**, 377 (1979); J. R. Comfort, Sam M. Austin, P. J. Debevec, G. L. Moake, R. W. Finlay, and W. G. Love, Phys. Rev. C **21**, 2174 (1980); J. R. Comfort, G. L. Moake, C. C. Foster, P. Schwandt, C. D. Goodman, J. Rapaport, and W. G. Love, *ibid.* **24**, 1834 (1981); J. R. Comfort, R. E. Segel, G. L. Moake, D. L. Miller, and W. G. Love, *ibid.* **23**, 1858 (1981).
[6] W. G. Love and M. A. Franey, Phys. Rev. C **24**, 1073 (1981).
[7] M. A. Franey and W. G. Love, Phys. Rev. C **31**, 488 (1985).
[8] S. Cohen and D. Kurath, Nucl. Phys. **73**, 1 (1965).
[9] D. J. Millener and D. Kurath, Nucl. Phys. **A255**, 315 (1975).
[10] K. J. Jones *et al.*, Phys. Rev. C **50**, 1982 (1994).
[11] R. de Swiniarski, D. L. Pham, and J. Raynal, Phys. Lett. B **213**, 247 (1988); Z. Phys. A **343**, 179 (1992).
[12] R. de Swiniarski, C. Glashausser, K. Jones, and D. L. Pham, submitted to Phys. Rev. C.
[13] Ch. Elster and P. C. Tandy, Phys. Rev. C **40**, 881 (1989); Ch. Elster, T. Cheon, E. F. Redish, and P. C. Tandy, *ibid.* **41**, 814 (1990), and references cited therein.
[14] T. Mefford, R. H. Landau, L. Berge, and K. Amos, Phys. Rev. C **50**, 1648 (1994); H. F. Arellano, F. A. Brieva, and W. G. Love, *ibid.* **41**, 2188 (1990); **42** 1782 (1990); C **43**, 2734 (1991).
[15] J. Raynal, computer code DWBA (NEA 1209/02).
[16] H. O. Meyer *et al.*, Phys. Rev. C **27**, 459 (1983); H. Seifert *et al.*, *ibid.* **47**, 1615 (1993), and references contained therein.
[17] R. A. Arndt, L. D. Roper, R. A. Brian, B. J. VerWest, and P. Signell, Phys. Rev. D **28**, 97 (1983); R. A. Arndt, J. S. Hyslop, and L. D. Roper, *ibid.* **35**, 128 (1987).
[18] M. Lacombe, B. Loiseau, J. M. Richard, R. Vinh Mau, J. Côté, P. Pirès, and R. de Tourreil, Phys. Rev. C **21**, 861 (1980).
[19] H. V. von Geramb, K. Amos, L. Berge, S. Bräutigam, H. Kohlhoff, and A. Ingermarsson, Phys. Rev. C **44**, 73 (1991).
[20] P. J. Dortmans and K. Amos, Phys. Rev. C **49** 1309 (1994).
[21] P. J. Dortmans and K. Amos, University of Melbourne Report No. UM-P-95/27, 1995 (unpublished).
[22] M. I. Haftel and F. Tabakin, Nucl. Phys. **A158**, 1 (1970).
[23] P. J. Dortmans and K. Amos, J. Phys. G **17**, 901 (1991).
[24] P. J. Dortmans, Ph.D. thesis, University of Melbourne, 1992 (unpublished).
[25] R. Machleidt, K. Hollinde, and Ch. Elster, Phys. Rep. **149**, 1 (1987).
[26] OXBASH-MSU (the Oxford-Buenos Aries-Michigan State University shell model code), A. Etchegoyen, W. D. M. Rae, and N. S. Godwin (MSU version by B. A. Brown, 1986); B. A. Brown, A. Etchegoyen, and W. D. M. Rae, MSUCL Report No. 524, 1986 (unpublished).
[27] F. Ajzenberg-Selove, Nucl. Phys. **A506**, 1 (1990).
[28] K. Amos, I. Morrison, R. Smith, and K. W. Schmid, Aust. J. Phys. **34**, 493 (1981).
[29] G. H. Neuschaefer, M. N. Stephens, S. L. Tabor, and K. W. Kemper, Phys. Rev. C **28**, 1594 (1983); K. W. Jones *et al.*, Phys. Lett. **128B**, 281 (1983).
[30] A. Yamaguchi, T. Terasawa, K. Nakahara, and Y. Torizuka, Phys. Rev. C **3**, 1750 (1971).
[31] D. J. Millener, private communication.
[32] E. Uegaki, Y. Abe, S. Okabe, and H. Tanaka, Prog. Theor. Phys. **57**, 1262 (1977); **62**, 1621 (1979).
[33] T. deForest, Jr. and J. D. Walecka, Adv. Phys. **15**, 1 (1966).
[34] J. L. Friar and W. C. Haxton, Phys. Rev. C **31**, 2027 (1985).

[35] S. Karataglidis, P. Halse, and K. Amos, Phys. Rev. C **51**, 2494 (1995).
[36] S. Karataglidis, University of Melbourne Internal Report No. UM-P-95/29 1995 (unpublished).
[37] K. Amos, R. de Swiniarski, and L. Berge, Nucl. Phys. **A485**, 653 (1988).
[38] J. M. Delbrouck-Habaru and Daniel M. Dubois, Comput. Phys. Commun. **8**, 396 (1974).
[39] J. A. Jansen, R. Th. Peerdeman, and C. de Vries, Nucl. Phys. **A188**, 337 (1972).
[40] I. Sick and J. S. McCarthy, Nucl. Phys. **A150**, 631 (1970).
[41] A. Nakada, Y. Torizuka, and Y. Horikawa, Phys. Rev. Lett. **27**, 745 (1971); **27**, 1102 (1971).
[42] J. B. Flanz, R. S. Hicks, R. A. Lindgren, G. A. Peterson, A. Hotta, B. Parker, and R. C. York, Phys. Rev. Lett. **41**, 1642 (1978).
[43] S. S. Avancini and E. J. V. de Passos, J. Phys. G **21**, 63 (1995).
[44] Hall Crannell, Phys. Rev. **148**, 1107 (1966).
[45] Y. Torizuka *et al.*, Phys. Rev. Lett. **22**, 544 (1969).
[46] J. B. Flanz, R. S. Hicks, R. A. Lindgren, G. A. Peterson, J. Dubach, and W. C. Haxton, Phys. Rev. Lett. **43**, 1922 (1979).
[47] W. H. Bassichis, A. L. Kerman, and J. P. Svenne, Phys. Rev. **160**, 746 (1967).
[48] C. W. De Jager, H. De Vries, and C. De Vries, At. Data Nucl. Data Tables **14**, 479 (1974).
[49] J. Raynal, Nucl. Phys. **A97**, 572 (1967); Notes On DWBA91, CEN-Saclay report, 1991 (unpublished).
[50] H. V. von Geramb and K. Amos, Nucl. Phys. **A163**, 337 (1970).